AAC Journals.ASM.org

Relative to Quinine and Quinidine, Their 9-Epimers Exhibit Decreased Cytostatic Activity and Altered Heme Binding but Similar Cytocidal Activity versus *Plasmodium falciparum*

Alexander P. Gorka,[a,b,c] Katy S. Sherlach,[a,b,c] Angel C. de Dios,[c] Paul D. Roepe[a,b,c]

Department of Biochemistry and Molecular & Cellular Biology,[a] Center for Infectious Disease,[b] and Department of Chemistry,[c] Georgetown University, Washington, DC, USA

The 9-epimers of quinine (QN) and quinidine (QD) are known to exhibit poor cytostatic potency against *P. falciparum* (Karle JM, Karle IL, Gerena L, Milhous WK, Antimicrob. Agents Chemother. 36:1538–1544, 1992). We synthesized 9-*epi*-QN (eQN) and 9-*epi*-QD (eQD) via Mitsunobu esterification-saponification and evaluated both cytostatic and cytocidal antimalarial activities. Relative to the cytostatic activity of QN and QD, we observed a large decrease in cytostatic activity (higher 50% inhibitory concentration [IC_{50}s]) against QN-sensitive strain HB3, QN-resistant strain Dd2, and QN-hypersensitive strain K76I, consistent with previous work. However, we observed relatively small changes in cytocidal activity (the 50% lethal dose), similar to observations with chloroquine (CQ) analogues with a wide range of IC_{50}s (see the accompanying paper [A. P. Gorka, J. N. Alumasa, K. S. Sherlach, L. M. Jacobs, K. B. Nickley, J. P. Brower, A. C. de Dios, and P. D. Roepe, Antimicrob. Agents Chemother. 57:356–364, 2013]). Compared to QN and QD, the 9-epimers had significantly reduced hemozoin inhibition efficiency and did not affect pH-dependent aggregation of ferriprotoporphyrin IX (FPIX) heme. Magnetic susceptibility measurements showed that the 9-epimers perturb FPIX monomer-dimer equilibrium in favor of monomer, and UV-visible (VIS) titrations showed that eQN and eQD bind monomer with similar affinity relative to QN and QD. However, unique ring proton shifts in the presence of zinc(II) protoporphyrin IX (ZnPIX) indicate that binding of the 9-epimers to monomeric heme is via a distinct geometry. We isolated eQN- and eQD-FPIX complexes formed under aqueous conditions and analyzed them by mass, fluorescence, and UV-VIS spectroscopies. The 9-epimers produced low-fluorescent adducts with a 2:1 stoichiometry (drug to FPIX) which did not survive electrospray ionization, in contrast to QN and QD complexes. The data offer important insight into the relevance of heme interactions as a drug target for cytostatic versus cytocidal dosages of quinoline antimalarial drugs and further elucidate a surprising structural diversity of quinoline antimalarial drug-heme complexes.

Malaria remains a very serious threat to global health, affecting hundreds of millions of people and killing approximately 1 million annually (1). Five species of *Plasmodium* cause disease in humans, with *Plasmodium falciparum* being the most lethal (2). Given the growing spread of resistance to current antimalarial drugs and the lack of an effective vaccine (1–4), development of novel, cost-effective, and efficacious drugs is of utmost importance. A vital component to new drug development is elucidating the molecular mechanism of effective antimalarial drugs as well as the mechanism(s) of parasite drug resistance. Further improvement to quinoline-based antimalarials has historically focused on modification of the 4- and 8-aminoquinolines, whereas synthesis of quinine (QN) derivatives has largely been avoided due, in part, to toxicity concerns and complexities in chemical synthesis (5).

Yet QN, a quinoline methanol natural product from the bark of the *Cinchona* tree (4), has been used as an effective antimalarial drug for centuries, and QN resistance (QNR) remains relatively low. Correspondingly, QN is currently a WHO-recommended therapy for some chloroquine (CQ)-resistant (CQR) and artemisinin (ART)-resistant *P. falciparum* infections. Despite long-term use and important activity against drug-resistant malaria, the molecular mechanism of action of QN has not yet been fully elucidated. Understanding similarities versus differences relative to CQ would assist with the additional development of effective quinoline antimalarial drugs.

Similar to CQ and other quinoline-based antimalarial drugs, QN is believed to inhibit heme detoxification within the digestive vacuole (DV) of the parasite, by inhibiting the crystallization of toxic ferriprotoporphyrin IX (FPIX) heme to nontoxic hemozoin via binding to the precrystalline monomeric and/or dimeric form of heme (6–10). Resistance to QN is multifactorial and in various studies has been linked to mutations and/or overexpression of several genes, including those encoding the *P. falciparum* chloroquine resistance transporter (PfCRT) (11, 12), multidrug resistance protein (PfMDR1) (13), and Na^+/H^+ exchanger (PfNHE) (14). One theory for why QN remains active against some CQR phenotypes is that certain mutant PfCRT isoforms that confer reduced CQ accumulation via increased PfCRT-mediated transport of CQ do not accommodate increased transport of QN, even though CQ and QN are structurally similar (15–17). We have recently discovered that the mechanism of resistance to the cytocidal (cell-killing) activity of CQ is likely distinct from the mechanism of resistance to the cytostatic (growth-inhibitory) activity

Received 15 June 2012 Returned for modification 27 September 2012
Accepted 26 October 2012
Published ahead of print 31 October 2012
Address correspondence to Paul D. Roepe, roepep@georgetown.edu.
Supplemental material for this article may be found at http://dx.doi.org/10.1128/AAC.01234-12.

doi:10.1128/AAC.01234-12

of CQ (16, 18, 19; see also the accompanying paper [20]). Other than one recent report (19), there has been no quantification of the 50% inhibitory concentration (IC_{50}) (cytostatic) versus the 50% lethal dose (LD_{50}) (cytocidal) for QN and its stereoisomers; therefore, it is currently not known how these parameters differ for various strains and isolates of *P. falciparum*.

The behavior of QN stereoisomers is particularly interesting and is in theory a quite useful tool for elucidating QN pharmacology. Karle and coworkers reported that while QN (8*S*,9*R*) and its 8,9-diastereomer quinidine (QD) (8*R*,9*S*) potently inhibit the growth of malarial parasites, 9-*epi*-QN (eQN) (8*S*,9*S*) and 9-*epi*-QD (eQD) (8*R*,9*R*) do not, showing strongly elevated IC_{50}s against CQ-sensitive (CQS) strain D6 and CQR strain W2 (21). Curiously, W2 was found to be approximately 3-fold more sensitive to eQN and eQD than D6. Albeit under nonphysiological conditions, Egan et al. demonstrated that the 9-epimers inhibit hemozoin formation less well *in vitro* than QN and QD (9). These findings, along with structural analysis of the compounds, led Karle et al. to hypothesize that the altered orientation of intermolecular hydrogen bonds with cellular receptor sites for the *threo* alkaloids eQN and eQD relative to that of their *erythro* counterparts, QN and QD (21), reduces *Cinchona* alkaloid potency. Recent work (6, 8, 10, 11, 13–17, 22) has suggested that the cellular receptor sites alluded to by Karle et al. may be one or more forms of free FPIX heme within the DV. Warhurst and coworkers investigated the physicochemical properties of the *erythro* versus *threo* isomers and calculated that the latter have an elevated aliphatic N pK_a (9.5 versus 8.6 for the *erythro* isomer) and a reduced log *D* at pH 7.4, predicting decreased membrane transfer (22). Thus, intrinsic differences in the antiplasmodial activities of the isomer pairs may result from (i) a different chemical interaction(s) with heme, (ii) a decreased ability of eQN and eQD to partition from aqueous to lipid phase (i.e., to cross membranes) (22), or (iii) perhaps altered binding to other (nonheme) cellular receptors. In parasites that are resistant to quinoline drugs, mutations in DV membrane transporters with stereospecific drug interactions (13, 15–17) might be predicted to further affect 9-epimer activity for these QNR or CQR strains.

To further distinguish between these possibilities, we hypothesized, based on a recent model for QN-heme adducts (6), that it is possible that the lack of hemozoin inhibition by eQN and eQD is due to altered monomeric heme binding arising from the change in configuration at the 9-position carbon. Consistent with solution and solid-state nuclear magnetic resonance (NMR) data, Alumasa and coworkers recently suggested that QN forms a highly fluorescent 1:1 complex with FPIX through a dative Fe—O interaction which is stabilized by an intramolecular five-membered ring formed via hydrogen bonding between the hydroxyl proton and quinuclidine nitrogen (6). Alumasa et al. also showed that, in solution, QN and QD bind to monomeric FPIX with high affinity and perturb the FPIX monomer-dimer equilibrium in favor of monomer (6).

We performed similar *in vivo* and *in vitro* experiments with the isomeric pairs to further elucidate *Cinchona* alkaloid antiplasmodial activity and resistance. We also measured the cytostatic (IC_{50}) and cytocidal (LD_{50}) activities for QN-susceptible (QNS) versus QNR strains, hemozoin inhibitory activities, heme binding affinity, magnetic moment for drug-heme solutions, drug effects on pH-dependent heme aggregation, and heme ring current effects on bound drug. We isolated eQN- and eQD-heme complexes formed in aqueous solution and determined their stoichiometry and fluorescence properties. In sum, the data elucidate key differences in heme interactions for the isomeric pairs, suggest a novel model for eQN and eQD complexation with heme, and shed light on the relevance of heme interactions for the cytostatic versus cytocidal activities of the *Cinchona* alkaloids.

MATERIALS AND METHODS

Materials and chemicals. Routine chemicals, media, and solvents were reagent grade or better, purchased from Sigma-Aldrich (St. Louis, MO) or Fisher Scientific (Newark, DE), and used without further purification, unless otherwise noted. Sterile polystyrene 96-well tissue culture plates and other laboratory plastics were purchased from Fisher Scientific (Newark, DE). Kieselgel 60 silica was purchased from Selecto Scientific (Suwanee, GA). Sodium dodecyl sulfate (SDS) was purchased from Bio-Rad Laboratories (Hercules, CA). Hemin was from Fluka (Buchs, Switzerland). D_2O, dimethyl sulfoxide *d6* (DMSO-*d6*), and $CDCl_3$ were purchased from Cambridge Isotope Laboratories Inc. (Andover, MA). Zinc(II) protoporphyrin IX (ZnPIX) was purchased from Frontier Scientific (Logan, UT). SYBR green I nucleic acid dye was purchased from Invitrogen (Eugene, OR).

Antimalarial drugs QN monohydrochloride dihydrate, QD hydrochloride monohydrate, CQ diphosphate, and amodiaquine (AQ) dihydrochloride dihydrate were purchased from Sigma-Aldrich (St. Louis, MO). eQN and eQD were synthesized as described below. Synthesis of cinchonine analog 2 (CN-2) CN-4, QD analog 2 (QD-2), QN analog 8 (QN-8), and QN-12 was reported previously (23). The structures of all drugs used in this study are shown in Fig. 1.

General methods. Flash chromatography was performed on Kieselgel 60 (particle size, 0.032 to 0.063 mm). Thin-layer chromatography (TLC) analyses were performed on Selecto Scientific flexible TLC plates (silica gel 60, F 254, 200 μm). NMR spectra were obtained on a 400-MHz (^1H) and 100-MHz (^{13}C) Varian Fourier transform (FT)-NMR spectrometer (Santa Clara, CA) using $CDCl_3$ as the solvent, unless otherwise indicated, and using tetramethylsilane (TMS) as the external standard. Mass spectroscopic (MS) measurements were performed in methanol (MeOH) or acetonitrile (ACN) on a Varian 500 mass spectrometer equipped with an electrospray ionization (ESI) source. The electrospray needle was operated at 5 kV using N_2 as both the nebulizing gas (35 lb/in^2) and the drying gas (350°C, 10 lb/in^2). Sample was delivered using a syringe pump employing a gas-tight 1-ml syringe at a constant flow rate of 200 μl/min. Optical rotation (α) was measured at 589 nm (sodium D line) in ethanol (EtOH; 1-mg/ml solution) on a Rudolph Instruments DigiPol-DP781-TDV polarimeter (Denville, NJ) at room temperature using a 1-dm cell. Melting point analysis was performed on a Barnstead electrothermal manual MelTemp apparatus.

Synthesis of eQN and eQD. (*S*)-(6-Methoxyquinolin-4-yl) [(2*S*,4*S*,8*R*)-8-vinylquinuclidin-2-yl]methanol (eQN) and (*R*)-(6-methoxyquinolin-4-yl) [(2*R*,4*S*,8*R*)-8-vinylquinuclidin-2-yl]methanol (eQD) were prepared by one-pot Mitsunobu esterification-saponification (24). A stirred solution of QN or QD (500 mg, 1.5 mmol, 1.0 equivalent), triphenylphosphine (Ph_3P; 525 mg, 2.0 mmol, 1.3 equivalents), and *p*-nitrobenzoic acid (PNBA; 284 mg, 1.7 mmol, 1.1 equivalents) in anhydrous tetrahydrofuran (THF; 15 ml) was cooled to 0°C in an ice water bath, and diisopropyl azodicarboxylate (DIAD, 0.33 ml, 1.7 mmol, 1.1 equivalents) was added dropwise. The resulting mixture was stirred at 0°C for 20 min, allowed to warm gradually to room temperature, and stirred for an additional 3 h. After cooling to 0°C, lithium hydroxide (LiOH; 1 M, 10 ml) and MeOH (2 ml) were added, the solution was gradually warmed to room temperature again, and the reaction mixture was stirred for 12 h more. Organic solvents were removed *in vacuo*, and the residue was quenched with water (10 ml) and extracted with dichloromethane (CH_2Cl_2; 50 ml). The organic phase was separated, washed with saturated brine, and dried over anhydrous sodium sulfate, and the solvent was removed *in vacuo* to afford the crude product as a yellow oil. This was further purified by flash chromatography over silica using an initial $CHCl_3$-diethyl ether (3:1)

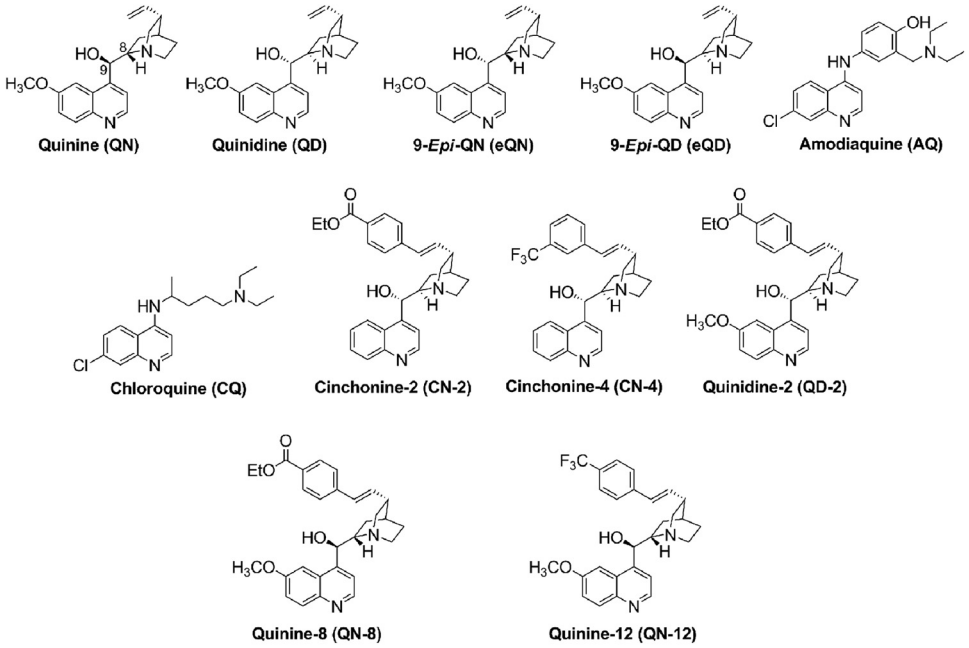

FIG 1 Structures of drugs used in this study. Positions 8 and 9 on the QN pharmacophore are highlighted. EtO indicates that an ethyl ester resides at that carbon ($-OC_2H_5$).

mobile phase followed by $CHCl_3$-MeOH-triethylamine (40:1:4) for product elution. The pure product was obtained as an off-white solid in 28% (eQN) or 31% (eQD) yield.

eQN. ^{1}H NMR ($CDCl_3$; 400 MHz; m, multiplet; s, singlet; d, doublet; dd, doublet of a doublet) δ 1.00 (m, 1H), 1.26 (m, 1H), 1.51 (m, 1H), 1.70 (m, 3H), 2.40 (s, 1H), 2.89 (m, 2H), 3.38 (m, 3H), 3.95 (s, 3H), 5.00 (m, 2H), 5.16 (d, J = 10 Hz, 1H), 5.72 (m, 1H), 7.37 (dd, J = 2.8 Hz, J = 9.2 Hz, 1H), 7.40 (d, J = 4.4 Hz, 1H), 7.68 (d, J = 2.8 Hz, 1H), 8.02 (d, J = 9.2 Hz, 1H), 8.72 (d, J = 4.4 Hz, 1H); ^{13}C NMR ($CDCl_3$, 100 MHz) δ 24.7, 27.0, 27.1, 29.6, 39.1, 40.9, 55.3, 55.7, 61.6, 70.7, 102.5, 115.3, 120.1, 121.5, 128.0, 131.6, 140.3, 143.9, 144.8, 147.5, 157.6; melting point, 183 to 185°C; $[\alpha]^{22D}$ (EtOH) +23 (*c* 1.0); MS (ESI) *m/z* calculated for $C_{20}H_{24}N_2O_2$: 324.18. Found $(M + H)^+$: 325.1.

eQD. ^{1}H NMR ($CDCl_3$, 400 MHz) δ 1.04 (m, 1H), 1.32 (m, 1H), 1.60 (m, 2H), 1.72 (s, 1H), 2.35 (m, 1H), 3.02 (m, 6H), 3.93 (s, 3H), 5.13 (m, 3H), 5.89 (m, 1H), 7.36 (dd, J = 2.8 Hz, J = 9.2 Hz, 1H), 7.48 (d, J = 4.4 Hz, 1H), 7.58 (d, J = 2.4 Hz, 1H), 8.02 (d, J = 9.2 Hz, 1H), 8.74 (d, J = 4.4 Hz, 1H); ^{13}C NMR ($CDCl_3$, 100 MHz) δ 23.9, 26.4, 27.3, 38.7, 46.8, 49.1, 55.4, 62.4, 69.8, 101.9, 115.0, 120.0, 121.7, 128.0, 131.6, 139.8, 144.7, 144.8, 147.5, 157.5; melting point, 185 to 187°C; $[\alpha]^{22D}$ (EtOH) +75 (*c* 1.0); MS ESI *m/z* calculated for $C_{20}H_{24}N_2O_2$: 324.18. Found $(M + H)^+$: 325.0.

Antiplasmodial activity measurements. *P. falciparum* strains HB3 and Dd2 were obtained from the Malaria Research and Reference Reagent Resource Center (Manassas, VA). *P. falciparum* strain K76I was a generous gift of Roland Cooper (Dominican University of California, San Rafael, CA). Off-the-clot, heat-inactivated pooled type O-positive human serum and type O-positive human whole blood were purchased from Biochemed Services (Winchester, VA). Custom 5% O_2–5% CO_2–90% N_2 culturing gas blend was purchased from Robert's Oxygen (Rockville, MD).

All *P. falciparum* strains were maintained using the method of Trager and Jensen (25) with minor modifications. Briefly, cultures were maintained under an atmosphere containing 5% CO_2, 5% O_2, and 90% N_2 gaseous mix at 2% hematocrit and 1 to 2% parasitemia in RPMI 1640 supplemented with 10% type O-positive human serum, 25 mM HEPES (pH 7.4), 23 mM $NaHCO_3$, 11 mM glucose, 0.75 mM hypoxanthine, and 20 μg/liter gentamicin with regular medium changes every 48 h. Antiplasmodial cytocidal and cytostatic activity was assessed against the CQS HB3 strain, CQR Dd2 strain, and CQR K76I line (11, 12), as previously described (19, 26), with minor modifications. The cytocidal assay utilizes a 6-h bolus dose with high concentrations of drug, followed by washing drug away and growth in the absence of drug for 48 h, while the cytostatic assay utilizes continuous growth for 48 h in the constant presence of low concentrations of drug. Test compounds were dissolved in deionized water, 50% EtOH, or DMSO. Serial drug dilutions were made using complete medium, and 100-μl aliquots were transferred to 96-well clear-bottom black plates. Following addition of 100 μl of asynchronous or sorbitol-synchronized culture (1% final parasitemia, 2% final hematocrit), plates were transferred to an airtight chamber gassed with 5% CO_2–5% O_2–90% N_2 and incubated at 37°C.

For the cytocidal assay, plates were incubated for 6 h, followed by centrifugation with an Eppendorf 5804 centrifuge fitted with an A-2-DPW rotor (Hauppauge, NY) at 700 × *g* for 3 min. Drug-containing medium was removed, and cell pellets were washed three times with 200 μl of complete medium per wash, using the same centrifuge settings, and resuspended in the same volume of medium. Washed plates along with the cytostatic assay plates were incubated at 37°C for 48 h. After 48 h, 50 μl of 10× SYBR green I dye (diluted using complete medium from a 10,000× DMSO stock) was added and plates were incubated for an additional 1 h at 37°C to allow DNA intercalation. Fluorescence was measured at 538 nm (485-nm excitation) using a Spectra GeminiEM plate reader (Molecular Devices, Sunnyvale, CA) fitted with a 530-nm long-pass filter. Linear standard curves of measured fluorescence versus known parasitemia were prepared immediately prior to plate analysis. Background controls included fluorescence from uninfected red blood cells. Data were analyzed using the Microsoft Excel 2007 program, and IC_{50} and LD_{50} values were obtained from sigmoidal curve fits to percent growth/survival-versus-drug concentration data using SigmaPlot (version 11.0) software. Reported values are the averages of three independent assays, with each assay conducted in triplicate (nine determinations total) and reported ± the standard error of the mean (SEM).

β-Hematin crystallization inhibition. β-Hematin crystal growth inhibition under physiological conditions in the presence of lipid catalyst

was assessed using a modified 96-well-plate high-throughput assay (see the accompanying paper [20]). Briefly, the assay uses physiological temperature and lipid catalyst and relies on the differential solubility properties of crystalline and noncrystalline forms of FPIX in 2.5% SDS (86.7 mM) and alkaline bicarbonate buffer (0.1 M, pH 9.1) to quantify crystallized heme. Hemin was dissolved in 0.1 M NaOH to 2 mM, 10 μl was transferred to each well of a 96-well plate, and propionate buffer (180 μl at the desired pH) plus 10 μl of sonicated phosphatidylcholine suspension (10 mg/ml) were then added (final FPIX heme concentration, 100 μM). Drugs at different concentrations were then added, the contents of the plates were mixed, and the plates were wrapped in plastic wrap and incubated at 37°C for 16 h. The assay was terminated by the addition of 100 μl of a solution of SDS dissolved in 0.1 M bicarbonate buffer (pH 9.1; final SDS concentration per well, 86.7 mM). The well contents were gently mixed, and the plate was incubated at room temperature for 10 min to allow undissolved hemozoin crystals to settle. A 50-μl aliquot from each well was then transferred to a second plate preloaded with 200 μl of SDS solution (86.7 mM) in 0.1 M bicarbonate buffer (pH 9.1). The absorbance of noncrystallized heme was recorded at 405 nm using a 96-well-plate-adapted ELx800 BioTek absorbance microplate reader (Winooski, VT). Standard curves of known heme concentration in the same solvent were generated for each assay and fit with a linear regression. Free heme remaining in solution (the inverse of the amount of hemozoin produced) was quantified using equation 1:

$$[H^X] = \left\{ \frac{\left(A^s_{405} - A^0_{405}\right) - C}{\varepsilon_{405}} \right\} \times D \qquad (1)$$

where $[H^X]$ is the concentration of heme (μM) remaining, A^s_{405} and A^0_{405} are the absorbances at 405 nm (average from triplicate wells) of the sample and blank, respectively, ε_{405} is the extinction coefficient for heme, C is a constant obtained from the fit to the calibration curve, and D is the dilution factor. Data were analyzed using the Microsoft Excel 2007 program, and β-hematin IC_{50}s were obtained from sigmoidal curve fits to percent crystal growth inhibition-versus-drug concentration data using the SigmaPlot (version 11.0) software. Reported values are the averages of three independent assays, with each assay conducted in triplicate (nine determinations total) and reported ± SEM.

Heme affinity measurements. Drug-heme affinity measurements were performed by monitoring the changes in the absorbance of the Soret band of heme in the presence of increasing concentrations of drug. Hemin was dissolved in DMSO or 0.1 M NaOH to 5 mM, followed by serial dilution to 5 μM in 40% DMSO–0.2 M HEPES (pH 7.4) for measuring binding to monomer (27). Drug solutions were prepared by dissolving the compound in DMSO and diluting to 3 mM in 40% DMSO–0.02 M HEPES (pH 7.4). A cuvette containing 3 ml of freshly prepared heme (5 μM) was titrated with increasing concentrations of drug (final concentration, 0 to 210 μM), the sample was mixed following each addition, and the absorbance of heme at 402 nm was recorded using an Agilent 8453 UV-visible (VIS) spectrophotometer (Santa Clara, CA). Solvent dilution controls were similarly performed (final volume dilution, 6.54%) using the relevant drug-free medium. Spectral and data analyses were performed using Kaleida Graph and SigmaPlot (version 11.0) software. Nonlinear least-squares curve fitting of the raw data was done using the Levenberg-Marquardt algorithm (7, 28) (initial affinity coefficient [K_a] input, 0.01 μM^{-1}) and K_as were computed.

Heme aggregation studies. The effect of various drugs on the pH-dependent solubility of FPIX was measured as previously performed (29), with minor modification. Briefly, drug stocks were prepared in 24 mM morpholineethanesulfonic acid (MES)-Tris buffer–0.1 M NaCl (pH 6.6) to a concentration of 1 mM. Hemin was dissolved in 0.1 M NaOH to 18 mM. Test solutions were prepared by combining 20 μl of drug, 10 μl of FPIX, and 980 μl of 24 mM MES-Tris buffer–0.1 M NaCl at the desired pH, for final drug and FPIX concentrations of 20 μM and 178 μM, respectively. Samples were mixed and incubated at room temperature for 30 min. Aggregated FPIX was pelleted by centrifugation at $1.61 \times 10^4 \times g$ for 3 min using an Eppendorf 5415 D microcentrifuge (Hauppauge, NY). The supernatant was removed and added to a 96-well plate containing 24 mM MES-Tris buffer–0.1 M NaCl (pH 6.6), resulting in a 1:4 (vol/vol) dilution. A standard curve of known heme concentration was generated for each assay. The absorbance at 405 nm was measured using a 96-well-plate-adapted ELx800 BioTek absorbance microplate reader (Winooski, VT). Data were analyzed using the Microsoft Excel 2007 program, and the pH at half FPIX solubility ($pH_{1/2}$) was extracted from sigmoidal curve fits to FPIX concentration-versus-pH data using SigmaPlot (version 11.0) software. Values are averages of three replicates, each performed in triplicate (nine determinations total), and are reported ± SEM.

Formation and analyses of aqueous drug-heme complexes. Drug-heme complexes formed under aqueous conditions were prepared as previously described for similar experiments (6). Hemin was dissolved in 0.1 M NaOH to give a 2 mM stock, and drug (100 mM in deionized water) was titrated into this solution while monitoring the pH. At a pH of ~8.5, copious heme was observed to precipitate, leaving a colorless solution of residual QN. The precipitate was isolated via vacuum filtration, washed with 0.1 M phosphate buffer (pH 7.0) to remove uncomplexed drug and heme, and dried under high vacuum to afford the complex as a dull green or dull gray powder.

Mass spectrometry analyses using a Varian 500 MS were performed by dissolving the precipitate in ACN. Fluorescence spectra were recorded from 5 μM samples dissolved in 1:1 MeOH–0.2 M HEPES (pH 7.2) using a Photon Technology International QuantaMaster 40 fluorometer (Birmingham, NJ) at 371 nm (334 nm excitation) using 1- and 2-nm slit widths. Spectra were processed using the Felix GX (version 4.0.3) and the Microsoft Excel 2007 programs.

Adduct stoichiometry was measured by dissolving each complex in 100% MeOH (which completely dissociates the complex), 40% (vol/vol) DMSO–0.2 M HEPES, pH 7.2 (which completely dissociates the complex), or 100% ACN (in which the complex remains intact) and quantifying the concentration of drug and FPIX via UV-VIS at 325 and 402 nm, respectively. Calibration curves of drug and monomeric FPIX were prepared by serial dilution of a 10 mM stock in DMSO in 40% (vol/vol) DMSO–0.2 M HEPES (pH 7.2).

Drug self-association studies. The propensity for eQN and eQD to self-associate relative to QN and QD was measured in order to further probe heme interactions (30). Drug stocks were prepared in CD_3OD to a final concentration of 1 or 50 mM. A 1-ml aliquot of each stock was transferred to a 5-mm (outer diameter) NMR tube, and NMR measurements were made at 298 K on a Varian FT-NMR spectrometer operating at a proton frequency of 400 MHz. Chemical shifts were referenced to the residual methyl signal of CH_3OH at 3.29 ppm. Spectra were processed using MestReC (version 4.8.1.1) software (Santiago de Compostela, Spain), and chemical shift differences were calculated by subtracting the value for each resonance measured at 50 mM from the corresponding value measured at 1 mM.

Magnetic susceptibility measurements. Magnetic susceptibility measurements were performed as previously described (27) in 40% DMSO–0.1 M phosphate buffer (pH 7.0). Both hemin and drug stock solutions (20 mM) were prepared in 100% DMSO-*d6*. Test samples (40% [vol/vol] DMSO–0.1 M phosphate buffer at pH 7.0) were prepared by adding 200 μl of hemin and the corresponding test compound into a 1.5-ml microcentrifuge tube, followed by addition of 600 μl of 0.1 M phosphate buffer to give a 1:1 solution of both components at 4 mM. The pH of the resulting samples was taken to be the pH of the buffered aqueous medium measured at 25°C using an Accumet Basic AB15 pH meter. The samples were transferred into 5-mm NMR tubes fitted with coaxial inserts containing the test compound in a similar solvent system. Measurements were made with a Varian FT-NMR spectrometer with a proton frequency of 400 MHz, and data were analyzed using MestReC (version 4.8.6) software. Magnetic susceptibility was determined using the Evans method (31) employing equation 2, which is appropriate for a superconducting magnet at 298 K:

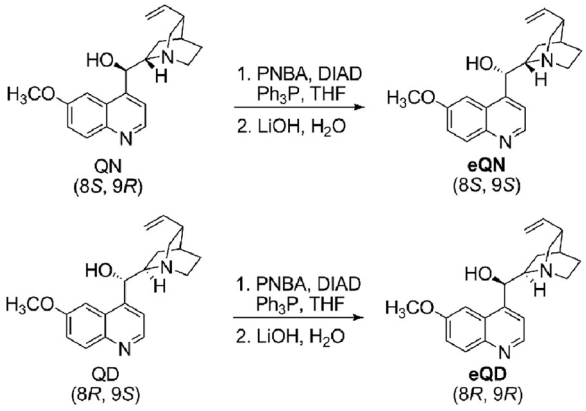

FIG 2 Synthesis of eQN and eQD via a one-pot Mitsunobu esterification-saponification of QN and QD (24).

$$\chi_m = \frac{-3\Delta\nu}{4\pi c} + \chi_D \quad (2)$$

where χ_m is the molar susceptibility of the paramagnetic substance (in cm^3/mol), $\Delta\nu$ is the chemical shift difference (in ppm) between a reference proton in the sample and that in a solution lacking the paramagnetic compound, c is the concentration of FPIX (in mol/ml), and χ_D is the diamagnetic susceptibility of heme (6.9×10^{-4} cgs units). Solvent susceptibility correction and the solution-solvent density differences are ignored. The molar susceptibility was converted to magnetic moment (μ) using equation 3, where T is the temperature (K):

$$\mu = 2.8\sqrt{\chi_m T} \quad (3)$$

Solution NMR experiments with ZnPIX. Solution NMR experiments using ZnPIX were conducted as previously described (6), with minor modification. ZnPIX and drug stock solutions were prepared at 10 mM in DMSO-*d6*. Drug-heme solutions (2:1; 3.334 and 1.667 mM, respectively) were then prepared and titrated to pH 7.0. Four hundred microliters of this solution was transferred to a microcentrifuge tube, followed by addition of 600 μl of D_2O. Thus, test samples contained a 2:1 drug-to-ZnPIX ratio in 40% DMSO-*d6*–D_2O. These solutions were transferred to 5-mm (outer diameter) NMR tubes for analysis, one-dimensional proton NMR spectra were recorded and analyzed as stated above, and chemical shifts were referenced to the residual DMSO peak.

RESULTS

Synthesis of eQN and eQD. Copious amounts of eQN and eQD were prepared via a one-pot Mitsunobu esterification-saponification reaction, as described previously (24). QN and QD were converted to the *p*-nitrobenzoate ester using *p*-nitrobenzoic acid and triphenylphosphine (oxidized to triphenylphosphine oxide via DIAD), followed by *in situ* saponification with lithium hydroxide, to afford eQN and eQD, respectively (Fig. 2), and purified (see Material and Methods).

Antiplasmodial activity. Cytostatic and cytocidal antiplasmodial activities against HB3 (QNS), Dd2 (QNR), and K76I (QN-hypersensitive) strains of *P. falciparum* were measured using the SYBR green I assay (26) (Table 1). Previously, strain K76I was found to be similarly CQR and QD resistant (QDR) relative to Dd2 (as defined by IC_{50} data) yet hypersensitive to QN, owing to a PfCRT mutation at position 76 (Dd2 harbors a K76T mutation) (11, 12). Similar to previous work (21), we found that eQN has an IC_{50} ~60-fold higher than that of QN against HB3 and ~10-fold higher than that of QN against Dd2. The IC_{50} of eQN for K76I was ~70-fold higher than that of QN, behavior that is more similar to that against HB3 than to that against Dd2. For eQD, the effects were more pronounced, with IC_{50} activities ~190-fold and ~25-fold higher than those of QD against HB3 and Dd2, respectively. For K76I, eQD had an IC_{50} ~10-fold higher than that of QD, behavior that is now more similar to that against Dd2 than to that against HB3 (e.g., the converse of the trend for eQN versus QN). Curiously, and as also found previously (21), Dd2 showed mild hypersensitivity to both eQN and eQD, and we found that relative to the sensitivity of HB3, strain K76I was even more hypersensitive to both 9-epimers than Dd2.

Importantly, however, these trends did not hold when potency was tabulated via cytocidal activity (LD_{50}; cf. Table 1). eQN showed LD_{50}s ~1.8-fold and ~1.2-fold higher than those of QN against HB3 and Dd2, respectively. eQD LD_{50}s were ~40-fold and ~1.2-fold higher than those of QD against HB3 and Dd2, respectively. Put another way, for any individual strain, the altered stereochemistry of the 9-epimers vastly decreased the cytostatic potency (changes IC_{50}) but (with one important exception for the IC_{50} of eQD versus that of QD against HB3) only mildly altered the cytocidal potency (LD_{50}). One interpretation is that the molecular targets for *Cinchona* alkaloid cytostatic and cytocidal activities must differ. Also, on the basis of the patterns for the QNR strains versus those for the hypersensitive strains, it also seems likely that mechanisms of cytostatic versus cytocidal resistance must differ.

Consistent with these conclusions, when defined by IC_{50}, strain K76I exhibited rather significant (≥8-fold) hypersensitivity to eQN and QN relative to that of HB3 but similar (<2-fold) differences in LD_{50}s for the same drugs relative to those for HB3 (Table 1). The QD-eQD pair displays a different trend. Relative to HB3, strain K76I showed mild (~3.5-fold) eQD hypersensitivity, as defined by IC_{50}, but 3-fold greater resistance, as defined by LD_{50}. Strain K76I was 5-fold more resistant to QD than HB3 via IC_{50} but an incredible 200-fold more resistant than HB3 via LD_{50}. See also

TABLE 1 Antiplasmodial IC_{50}s and LD_{50}s for QNS strain HB3, QNR strain Dd2, and the K76I strain[d]

Alkaloid	Experimental IC_{50} (nM)[a]					Experimental LD_{50} (μM)[a]				
	HB3	Dd2	R_f[b]	K76I	R_f[c]	HB3	Dd2	R_f[b]	K76I	R_f[c]
QN	107. 2 (12.4)	265.6 (14.6)	2.5	12.1 (0.9)	0.1	9.11 (0.4)	36.3 (0.9)	4.0	17.3 (0.9)	2.0
eQN	6,588.5 (358.2)	2,237.6 (76.4)	0.3	838.9 (64.5)	0.1	16.1 (1.6)	42.4 (0.5)	2.6	15.0 (1.0)	1.0
QD	41.9 (6.0)	147.2 (3.1)	3.5	209.5 (2.3)	5.0	0.4 (0.1)	33.6 (0.1)	77.7	105.6 (4.4)	244.3
eQD	7,893.6 (46.8)	3,588.3 (194.1)	0.5	2,175.6 (125.2)	0.3	17.6 (1.4)	39.8 (0.9)	2.3	49.6 (3.3)	3.0

[a] Experimental IC_{50} and LD_{50} values are averages of three independent measurements (9 replicates total), with SEMs reported in parentheses.
[b] R_f = Dd2 value/HB3 value.
[c] R_f = K76I value/HB3 value.
[d] The K76I strain is hypersensitive to QN but resistant to QD (11, 12, 15).

TABLE 2 β-Hematin inhibitory IC_{50} data at pH 5.2 and 5.6[a]

Alkaloid	β-Hematin IC_{50} (μM)	
	pH 5.2	pH 5.6
QN	255.4 (22.7)	42.5 (8.3)
eQN	>1,000	>3,000
QD	176.2 (4.9)	27.2 (2.7)
eQD	>1,000	>3,000

[a] Less than 10% inhibition is seen for the 9-epimers at 1 mM, leading to an estimated IC_{50} above several mM. Experimental IC_{50} and values are averages of three independent measurements (9 replicates total), with SEMs reported in parentheses.

references 11, 12, 15, 17, and 19 for selected quinoline activity data versus these strains.

Hemozoin inhibition. As mentioned above, inhibition of parasite hemozoin formation is believed to be the principal basis of antiplasmodial activity for quinoline drugs like the *Cinchona* alkaloids. However, this theory is based entirely on cytostatic activity (IC_{50}) data, since, with one exception (19), *in vitro* antiplasmodial activity is always routinely quantified via IC_{50}. While we indeed found that QN and QD actively inhibit the formation of hemozoin under physiological conditions in the low- to mid-μM range at both pH 5.2 and 5.6, eQN and eQD do not, with inhibitory IC_{50}s being above several mM (Table 2). We use measurement at both pH 5.2 and 5.6 to mimic variable physiological conditions, since different DV pHs for sensitive (HB3) versus resistant (Dd2) strains have been measured in some studies (32). These data suggest that the loss of cytostatic activity for the 9-epimers is due to an inability to prevent hemozoin formation, as also suggested by Egan et al. (9).

We next plotted the hemozoin (β-hematin) inhibitory IC_{50} (β-hematin inhibitory activity [BHIA]) against a series of QN analogues with variable cytostatic potency (23) to test for possible correlations (Fig. 3). The antiplasmodial IC_{50} was indeed mildly correlated with the BHIA IC_{50} across the series ($R^2 > 0.54$). However, interestingly, the correlation vanished when LD_{50} data were plotted ($R^2 < 0.01$; Fig. 3, caption). Consistent with the data in Table 1, this further suggests that *Cinchona* alkaloid targets for cytostatic versus cytocidal activities differ.

Heme binding affinity. As described below, the 9-epimers promote stabilization of monomeric heme (see "FPIX magnetic moment" below). Ideally, experiments to determine the affinity of the isomeric pairs for binding monomeric FPIX would be performed under physiologically relevant aqueous conditions. However, drug-heme titrations are performed in 40% aqueous DMSO due to the decreased intensity of the Soret band, less-than-strict adherence to Beer's law, insolubility, and potential for heme dimerization and aggregation outside these conditions (7, 27, 33). We found that eQN binds monomer with a similar affinity as QN; however, eQD binds with a ~5-fold lower K_a than QD (Fig. 4; Table 3).

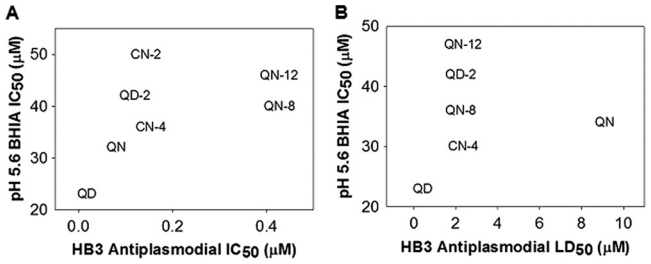

FIG 3 Antiplasmodial activity of a series of QN analogues (23). (A) BHIA IC_{50} versus antiplasmodial IC_{50}; (B) BHIA IC_{50} versus antiplasmodial LD_{50}. The IC_{50}s shown are averages of three independent measurements, each done in triplicate (9 replicates total) as reported previously (23). LD_{50} values are averages ± SEMs of three replicates and are as follows: CN-2, 2,337.9 ± 4.3 nM; CN-4, 2,360.6 ± 13.4 nM; QD-2, 2,234.1 ± 7.4 nM; QN-8, 2,251.4 ± 28.4 nM; QN-12, 2,346.5 ± 13.2 nM.

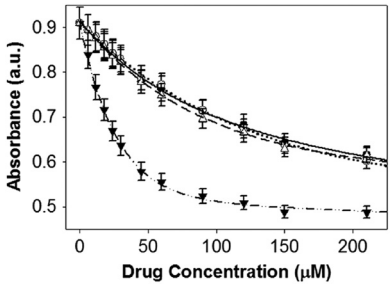

FIG 4 Drug-heme binding curves. Affinity was measured by titrating increasing concentrations of QN (●), eQN (○), QD (▼), and eQD (Δ) into a solution of monomeric FPIX, followed by nonlinear least-squares analysis (Levenberg-Marquardt algorithm [7, 28]) to determine K_a (Table 3; see Materials and Methods). a.u., absorbance units.

Heme aggregation effects. The effect of various drugs on the pH-dependent solubility of monomeric FPIX was measured by varying the pH versus a constant FPIX concentration (178 μM) and drug concentration (20 μM) (see reference 29 for a discussion of these aggregation phenomena and their presumed role in hemozoin formation). We found that eQN and eQD did not affect the pH-dependent solubility of FPIX, whereas QN, QD, CQ, and AQ produced a marked effect over a relatively narrow pH range (Fig. 5A; see also reference29). This effect is immediately apparent when the midpoints of each solubility curve are quantified (Fig. 5B).

Drug-heme adducts. We next isolated the eQN-, eQD-, QN-, and QD-monomeric FPIX complexes formed under aqueous conditions using methods published previously (6) and characterized their properties. Qualitatively, we found that the 9-epimer adducts are weaker than those formed with QN and QD, as evidenced by the ease of resolubilization in neutral buffer following precipitation and the fact that yields were significantly lower than those for QN and QD under the same conditions. The eQN- and eQD-FPIX adducts were also ~20- and 10-fold less fluorescent, respectively, than the QN- and QD-FPIX adducts (Fig. 6; Table 4).

TABLE 3 Drug-heme affinity coefficients for binding monomeric FPIX[b]

Alkaloid	Experimental K_a for monomer (M^{-1} [10^4])[a]	R^2
QN	0.75 (0.07)	1.00
eQN	0.61 (0.11)	1.00
QD	4.40 (0.04)	0.99
eQD	0.94 (0.10)	1.00

[a] Experimental K_a values are averages of three independent measurements (9 replicates total), with SEMs reported in parentheses.
[b] Drug-heme affinity coefficients for binding monomeric FPIX were obtained via nonlinear least-squares analysis of binding data using the Levenberg-Marquardt algorithm, which is described elsewhere (7, 28). See the caption to Fig. 4 for binding data.

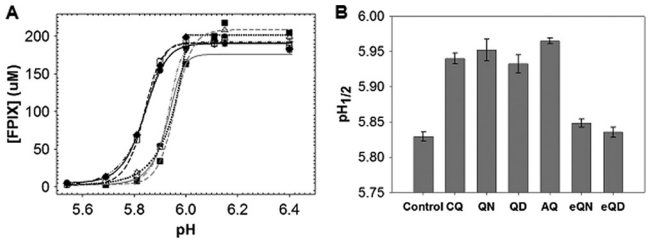

FIG 5 Drug effects on pH-dependent heme aggregation. (A) Concentration of free (nonaggregated) FPIX remaining in solution versus pH in the presence of no drug (●), CQ (○), QN (▼), QD (Δ), AQ (■), eQN (□), and eQD (◆); (B) the midpoint ($pH_{1/2}$) of each curve was calculated via sigmoidal regression.

ESI-MS analysis of the QN and QD complexes gave rise to peaks at *m/z* 325 and 616, corresponding to free QN H^+/QD H^+ and free FPIX monomer, respectively, and clear major peaks at *m/z* 938, 940, and 941 (Table 4; see Fig. S1 in the supplemental material). These findings coincide with the calculated *m/z* values of $(M - 2H)^+$ equal to 938.6, $(M)^+$ equal to 940.4, and $(M + H)^+$ equal to 941.4 for $C_{54}H_{55}FeN_6O_6$, corresponding to 1:1 drug-FPIX complexes (6). The 9-epimer adducts, however, did not survive electrospray ionization, as evidenced by peaks at *m/z* 325 and 616 only (Table 4; see Fig. S1 in the supplemental material), which again suggests that these are drug-heme complexes weaker than those formed by QN and QD (6).

We measured the drug-FPIX stoichiometry for each of the four complexes via UV-VIS titration (see Materials and Methods). Each adduct was dissolved in 100% methanol (which completely dissociates the complex), 40% (vol/vol) DMSO-HEPES (which completely dissociates the complex), or 100% acetonitrile (in which the complex remains intact), and three separate measurements for the concentration of drug and FPIX in each sample were performed at 325 and 402 nm, respectively. Interestingly, in spite of their weak nature, the results show that eQN and eQD adducts have a 2:1 stoichiometry (drug-FPIX), while QN and QD form 1:1 adducts (Table 4) (6).

Drug self-association. The propensity for eQN and eQD to self-associate, meaning that they form dimers through π-π interactions between the quinoline rings, was compared to that previously measured for QN and QD (30), to test whether an increased

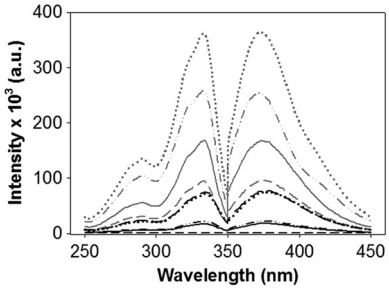

FIG 6 Fluorescence excitation and emission spectra for 5 μM QN-FPIX adduct (gray dotted line, top), QD-FPIX adduct (gray dash-dot-dot line, second from top), QD (gray continuous line, third from top), QN (gray dashed line, fourth from top), eQD (black dash-dot line, fifth from top), eQN (black dotted line, sixth from top), eQN-FPIX adduct (black dash-dot-dot line, seventh from top), eQD-FPIX adduct (black continuous line, eighth from top), and FPIX (black dashed line, bottom) performed in 1:1 methanol–0.2 M HEPES (pH 7.2) at an excitation λ of 334 nm and an emission λ of 371 nm.

TABLE 4 Drug-monomeric heme adduct properties

Species	Fluorescence maximum (10^3)[a]		Adduct stoichiometry[b] for drug-FPIX	ESI molecular ion(s) observed (*m/z*)[c]
	λ_{ex} (334 nm)	λ_{em} (371 nm)		
FPIX	1.13	1.15		616
QN-FPIX	360	363	0.9 (0.1)	325, 616, 938, 940, 941
eQN-FPIX	17.6	17.8	2.0 (0.3)	325, 616
QD-FPIX	255	256	1.2 (0.1)	325, 616, 938, 940, 941
eQD-FPIX	21.7	21.9	2.4 (0.1)	325, 616

[a] Data correspond to those in Fig. 6. λ_{ex} and λ_{em}, excitation and emission λ's maxima, respectively.
[b] Values are averages of measurements performed in methanol, acetonitrile, and 40% (vol/vol) DMSO–0.2 M HEPES (pH 7.2), with SEMs reported in parentheses.
[c] *m/z* 325, $(M + H)^+$ for QN or QD free base; *m/z* 616, $(M)^+$ for FPIX; *m/z* 938, 940, and 941, $(M - 2H)^+$, $(M)^+$, and $(M + H)^+$, respectively, for $C_{54}H_{55}FeN_6O_6$, corresponding to a 1:1 drug-heme complex. Peaks at *m/z* 498, 771, and 860 were also observed and were possible FPIX and adduct fragments. See also Fig. S1 in the supplemental material.

propensity for dimerization might explain the 2:1 drug-heme stoichiometry for the epimer-heme adducts. Chemical shifts of the quinoline protons were recorded at 1 mM and 50 mM concentrations, since if significant dimerization occurs, a chemical shift difference of ≥0.1 ppm is observed between each resonance at 1 and 50 mM (see reference 30 for a detailed description). The largest difference measured for the isomer pairs was 0.02 ppm, with most differences being <0.01 ppm (see Table S1 in the supplemental material). Importantly, then, chemical shift differences were nearly identical for each drug, indicating no difference in the dimerization behavior of the 9-epimers and that of QN and QD.

FPIX magnetic moment (μ). We measured the magnetic susceptibility of FPIX (4 mM) in the presence of each isomer (4 mM) in 40% DMSO-phosphate buffer (100 mM) at pH 7.0. These measurements distinguish between the monomeric and μ-oxo dimeric FPIX species due to the strong antiferromagnetic coupling between the two high-spin (spin $[S] = 5/2$) ferric ions afforded by the oxide bridge in the latter (27). Theoretically, the μ-oxo dimer exhibits a magnetic moment per iron of 1.7 μ_B (the theoretical value for $S = 1/2$), whereas the monomer gives 5.9 μ_B (the theoretical value for $S = 5/2$). Our results (Table 5) showed that FPIX has a magnetic moment of 5.33 μ_B in the presence of eQN and 5.45

TABLE 5 Changes in chemical shift and μ for ZnPIX and FPIX, respectively, in the presence of drug[d]

Compound	Change in chemical shift[a] (ppm) for the following proton[b]:						FPIX μ[c]
	2	3	5	6	7	8	
QN	0.02	0.04	−0.08		0.02	0.01	5.33
eQN	0.02	0.32	0.03		0.10	0.44	5.33
QD	0.02	0.03	−0.11		0.02	0.01	6.00
eQD	0.03	0.40	0.04		0.07	0.51	5.53
CQ	−0.19	−0.34	−0.10	−0.96		−0.28	2.41

[a] The chemical shift difference between the corresponding proton in the presence and absence of heme (ZnPIX in 40% DMSO-*d6*–D_2O, pH 7.0). The negative sign indicates an upfield shift relative to the pure drug.
[b] Quinoline protons are numbered according to the IUPAC numbering system of the corresponding carbon atoms (see Table S1 in the supplemental material).
[c] Measured in solution for FPIX in the presence of the corresponding drug.
[d] See Materials and Methods.

μ_B in the presence of eQD. This is in close agreement with the measured magnetic moment in the presence of QN and QD and characteristic of the high-spin monomeric species. In contrast, the presence of CQ results in a magnetic moment of 2.41 μ_B, which is characteristic of the low-spin dimeric species. Thus, similar to QN and QD, the 9-epimers stabilize monomeric heme but not dimeric heme.

Solution NMR experiments with ZnPIX. Finally, NMR studies using nonparamagnetic ZnPIX were used to further probe drug-monomeric heme interactions (see reference6). Clear perturbations in chemical shift for the quinoline protons in the presence versus absence of ZnPIX were found (Table 5). The magnitude and sign (upfield versus downfield) of these shifts illustrate different distances between the quinoline and porphyrin ring systems (6). As expected, relatively large upfield (negative) shifts for CQ aromatic protons indicate a short (approximately 3- to 4-Å) CQ-FPIX interplanar distance, as previously determined (6). QN and QD show very minor changes in chemical shift, suggesting a wider (6-Å) distance between the quinoline and porphyrin for these alkaloids, as previously determined (see references 6 and10). In contrast to CQ, QN, and QD, however, eQN and eQD exhibit quite large downfield (positive) shifts in quinoline protons 3, 7, and 8, suggesting a quite short drug-heme distance in an arrangement that allows significant deshielding of these specific quinoline nuclei. These distance constraints, combined with additional data presented above, suggest a model for epimer binding to monomeric heme that is described below.

DISCUSSION

Recent results from our laboratory have suggested the importance of distinguishing between cytostatic and cytocidal activity when characterizing antimalarial drug potency (19; see the accompanying paper [20]), and the present work further emphasizes this principle. Previously, we found that resistance to CQ is 10-fold higher for Dd2 than HB3 when measured by IC_{50} but 120-fold higher for Dd2 than HB3 when measured by LD_{50}, suggesting significantly altered pharmacology at the different dosages (19). The result was less dramatic for QN and QD, which show 2- and 7-fold increased resistance for Dd2 than HB3, respectively, when measured by IC_{50} and 4- and 60-fold increased resistance for Dd2 than HB3, respectively, when measured by LD_{50}. However, when combined with data obtained in this study, it has becoming increasingly clear that cytostatic and cytocidal targets for quinoline-based antimalarial drugs, including *Cinchona* alkaloids, likely differ and that mechanisms of resistance to agents with cytostatic versus cytocidal activities likely differ (16).

Similar to Karle et al. (21), we observed vast differences in IC_{50} activity between QN and QD and their 9-epimers, with the epimers showing significantly reduced potency (Table 1). In contrast, the activities measured by LD_{50} tell a different story. While eQN and eQD were less potent than QN and QD when measured by IC_{50}, for each strain, the fold differences in LD_{50} between the isomer pairs were far lower, and in some cases (e.g., strain K76I), the 9-epimer LD_{50}s were lower (they had higher cytocidal potency than QN and QD). We found that relative to strain HB3, strain Dd2 was resistant to QN and hypersensitive to eQN when potency was defined via IC_{50} but that the strain was resistant to both when potency was defined by LD_{50}. Overall, these observations and others lead to several major conclusions.

First, the large differences in IC_{50}s (but not LD_{50}s) observed for these isomers suggest (see also reference19) that the molecular mechanisms of resistance to the cytostatic and cytocidal effects of quinoline antimalarial drugs likely differ, which is consistent with conclusions from previous drug transport analyses (18). Cytostatic resistance to QN (i.e., elevated IC_{50}) is believed to be mediated at least in part by PfCRT and/or PfMDR1 mutations that alter electrochemical potential-driven DV transport of the protonated drug (13, 14, 16, 17). A lack of eQN cytostatic resistance in Dd2 (lower IC_{50} relative to that of HB3) is easily rationalized by the finding that stereochemically distinct eQN was not transported as well as QN by the Dd2 mutant PfCRT, since substrate recognition by transporters is often quite stereoselective (16). This is entirely consistent with key conclusions reached previously on the basis of the IC_{50} behavior for strain K76I (11, 12, 15). Namely, this strain harbors a mutant Dd2 PfCRT isoform, but with I replacing T at position 76, which then produces stereochemically distinct responses to quinoline drugs (e.g., QN versus QD; see references 11 12 for a complete discussion).

Second, we suggest that the highly altered cytostatic activities but more similar cytocidal activities of the 9-epimers relative to those of QN and QD indicate that the stereochemistry of the 9-epimers negatively affects the interaction with the predominant cytostatic (IC_{50}) target but does not necessarily affect the interaction with the predominant cytocidal (LD_{50}) target(s). Consistent with the hemozoin inhibition data presented here, as well as in other studies (8–10), we favor the interpretation that the predominant IC_{50} target for quinoline antimalarials is one or more forms of uncrystallized heme within the DV, specifically, monomeric FPIX heme in the case of QN and QD (6). This is consistent with perturbations of monomer-dimer ratios, binding behavior, both the reduced cytostatic potencies and the reduced hemozoin inhibition activity of the 9-epimers, and no effect on pH-dependent heme aggregation that is believed to facilitate hemozoin crystallization (29). We also show that while the 9-epimers are capable of binding monomeric FPIX, they do so with altered stoichiometry. The BHIA IC_{50}s versus antiplasmodial activities for a series of five structurally related QN analogs synthesized previously (23) shows a strong correlation with cytostatic potency but not cytocidal potency.

Third, these data suggest which DV species of heme are particularly relevant for forming hemozoin. At least three forms of free FPIX heme exist in the DV: monomer, μ-oxo dimer, and head-to-tail dimer. An unresolved issue is which species is more directly relevant for hemozoin formation and, hence, which interactions with which species might be the most important for quinoline drug cytostatic potency. The 9-epimers do not inhibit formation of hemozoin under physiological conditions, and although they promote the high-spin FPIX monomer in solution (Table 5) and form complexes with FPIX that precipitate from aqueous solution, they do not do so with the same affinity, stoichiometry, and fluorescence properties as the complexes formed with QN and QD. The former are qualitatively weaker and less favored, as evidenced by the ease of resolubilization in neutral buffer following precipitation and significantly lower yield. Moreover, the 9-epimer complexes do not survive electrospray ionization, leading to sole peaks corresponding to free drug and FPIX in the mass spectrum (Table 4; see Fig. S1 in the supplemental material). The 9-epimers also do not have a measureable effect on pH-dependent heme aggregation (Fig. 5). This is in agreement with the well-accepted concept that 4-quinolinemethanols interact more

weakly with heme and are less potent inhibitors of hemozoin formation than the 4-aminoquinolines. Strikingly, eQN and eQD form solution adducts with monomeric FPIX at a ratio of 2:1 (drug-FPIX), while QN and QD form 1:1 complexes that are less stable in solution. Taken together, these results suggest that heme monomers are the chemical form of heme that is the most relevant for hemozoin formation.

Fourth, spectroscopic data allow us to propose a logical model for 9-epimer binding to free heme. Previously, Alumasa et al. found that the QN-FPIX adduct was >5-fold more fluorescent than QN (heme is not fluorescent at the wavelengths used) (6), a result that we again observed for both QN- and QD-FPIX complexes. This is likely due to transition dipole ordering in the complex (6), the structure of which is proposed to form through a noncovalent interaction between the heme iron center and the hydroxyl oxygen of QN, stabilized by a hydrogen-bonded intramolecular 5-membered ring (Fig. 7, center). Given the stoichiometry and fluorescence properties that we observed for the QD-FPIX complex, it is expected to have a similar structure and geometry. In contrast, the 9-epimer complexes are significantly less fluorescent than free drug and over 10-fold less fluorescent than the corresponding QN and QD adducts. NMR experiments with ZnPIX also revealed that eQN and eQD exhibit heme interactions in solution that are distinctly different from those of QN, QD, and CQ (Table 5). The large downfield shifts observed for the quinoline protons indicate a close quinoline-porphyrin distance in an arrangement that allows deshielding of specific quinoline nuclei (such as a face-to-edge π-π interaction in which the quinoline moieties are oriented along the sides of the porphyrin). QN and QD show only minor shifts in the presence of ZnPIX, indicating a larger drug-heme distance and the Fe—O binding model reported previously (6). The large upfield shifts observed for CQ quinoline protons reveal a close quinoline-porphyrin distance in an arrangement that allows shielding of the nuclei (such as a π-π interaction in which the quinoline is oriented above the plane of the porphyrin) (10).

Taken together, the 2:1 (drug-FPIX) stoichiometry, Evans method data showing preferential binding to the monomer, a lack of drug self-association, low adduct fluorescence, and ZnPIX data suggest that eQN and eQD form complexes with monomeric FPIX via an H structure, where the vertical lines represent the quinoline moieties and the horizontal line represents FPIX (Fig. 7, top). Static quenching resulting from formation of such a complex would lead to the observed drop in fluorescence intensity. Binding of the drugs through a face-to-edge π-π interaction with the sterically less hindered sides of the porphyrin would give rise to the observed deshielding of the quinoline nuclei.

Caner et al. (34) suggest that the epi-isomers should be better able to form an intramolecular H-bonded 5-membered ring recently shown to be important for binding of QN to monomeric heme (6). We previously argued that the stability of this ring promoted binding to monomer, so if it is more stable for the epi-isomers, the 2:1 H model for epi-isomer binding might appear to be paradoxical. Importantly however, for QN and QD, upon formation of the ring, the two bulky groups (quinoline and quinuclidine) are on the same side of the molecule, which is not preferred for free drug; however, this leaves one face completely free for interacting with heme, and thus, the Fe—O interaction is formed (6). In the case of eQN and eQD, upon formation of the ring, the bulky groups are on opposite sides of the molecule, which is a hindrance when binding to heme via this geometry. Thus, the epimers must interact along the sides of the porphyrin. That is, bulky group positioning due to the intrinsic stereochemistry of the drugs and the resulting steric arrangements of the heme interaction drives differential complex formation.

The H model for 9-epimer binding is less stable than Fe—O dative adduct structures for QN and QD with FPIX (Fig. 7, center), consistent with the weak ability of the 9-epimer adducts to

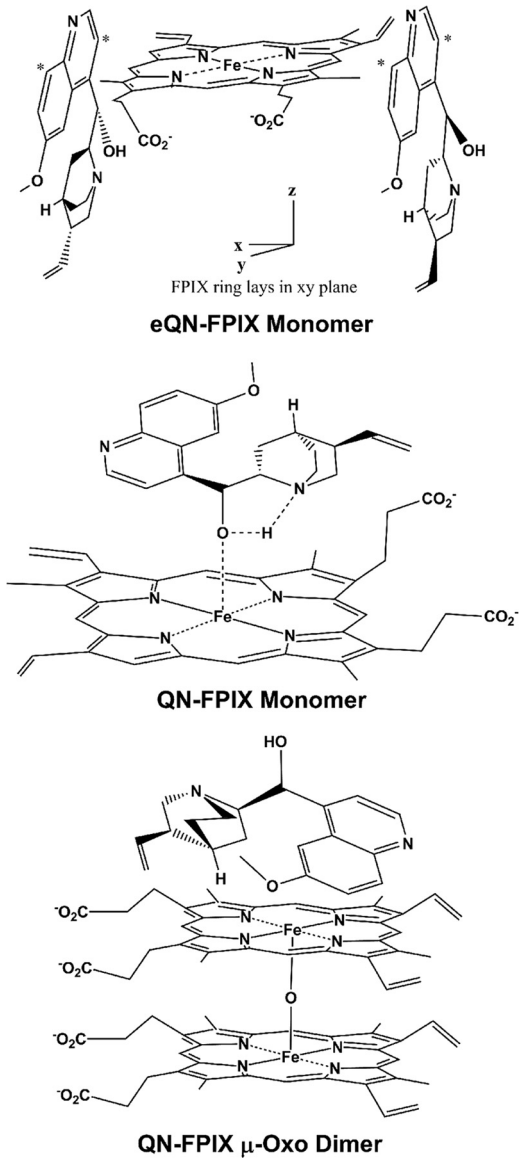

FIG 7 Proposed heme binding models. (Top) An eQN-monomer binding model based on stoichiometry, fluorescence, Evans (31), self-association, and ZnPIX data. The model suggests that eQN and eQD bind via face-to-edge π-π interactions between the least sterically hindered sides of the porphyrin and quinoline moieties. Those protons showing the greatest downfield shift (Table 5) are denoted with an asterisk and lie within the FPIX *x-y* plane. (Center) Previously determined QN-monomer structure (6). (Bottom) Previously determined QN–μ-oxo dimeric FPIX complex, which has been shown to form via face-to-face π-π interactions, with the quinoline system oriented above the vinyllic side of FPIX (10). QD complex structures are expected to be similar to the QN structures, and the eQD complex is expected to be similar to eQN-FPIX.

inhibit hemozoin formation. Similar to QN, the 9-epimers may also form complexes with μ-oxo dimeric heme (10) (Fig. 7, bottom). Regardless, the antiplasmodial, hemozoin inhibition, heme binding, heme aggregation, and Evans method data discussed above suggest that, for the QN isomer pairs, interaction with monomeric FPIX (and, thus, the monomeric adduct structure) is more important for hemozoin inhibition than interaction with μ-oxo dimeric FPIX. However, taken in their entirety, our data suggest that these structures are not as relevant for the cytocidal (parasite cell-killing) activity of *Cinchona* alkaloids as they are for cytostatic (growth-inhibition) activity. We suggest that for both QN analogues and CQ analogues (see the accompanying paper [20]), complete optimization of *in vivo* activity will require definition of their cytocidal targets, as well as the mechanism(s) of cytocidal drug resistance.

ACKNOWLEDGMENTS

We thank Jeremy Morgan and Theresa Dinio (University of North Carolina, Wilmington, NC) for providing QN structural analogs, Roland Cooper (Dominican University) for providing strain K76I, John Alumasa (The Pennsylvania State University) for helpful advice, Ansley Brown (University of South Florida Morsani College of Medicine) for technical assistance, and the Georgetown University Chemistry Department for synthetic chemistry support.

Financial support was received from NIH grant R0I AI056312.

REFERENCES

1. **World Health Organization.** 2010. World malaria report 2010. World Health Organization, Geneva, Switzerland. http://www.who.int/malaria/publications/atoz/9789241564106/en/index.html.
2. **Roepe PD.** 2009. Molecular and physiologic basis of quinoline drug resistance in *Plasmodium falciparum* malaria. Future Microbiol. **4**:441–455.
3. **Cheeseman IH, Miller BA, Nair S, Nkhoma S, Tan A, Tan JC, Al Saai S, Phyo AP, Moo CL, Lwin KM, McGready R, Ashley E, Imwong M, Stepniewska K, Yi P, Dondorp AM, Mayxay M, Newton PN, White NJ, Nosten F, Ferdig MT, Anderson TJ.** 2012. A major genome region underlying artemisinin resistance in malaria. Science **336**:79–82.
4. **Wells TN, Alonso PL, Gutteridge WE.** 2009. New medicines to improve control and contribute to the eradication of malaria. Nat. Rev. Drug Discov. **8**:879–891.
5. **Kumar V, Mahajan A, Chibale K.** 2009. Synthetic medicinal chemistry of selected antimalarial natural products. Antimicrob. Agents Chemother. **17**:2236–2275.
6. **Alumasa JN, Gorka AP, Casabianca LB, Comstock E, de Dios AC, Roepe PD.** 2011. The hydroxyl functionality and a rigid proximal N are required for forming a novel non-covalent quinine-heme complex. J. Inorg. Biochem. **105**:467–475.
7. **Egan TJ, Mavuso WW, Ross DC, Marques HM.** 1997. Thermodynamic factors controlling the interaction of quinoline antimalarial drugs with ferriprotoporphyrin IX. J. Inorg. Biochem. **68**:137–145.
8. **Egan TJ, Ncokazi KK.** 2005. Quinoline antimalarials decrease the rate of beta-hematin formation. J. Inorg. Biochem. **99**:1532–1539.
9. **Egan TJ, Ross DC, Adams PA.** 1994. Quinoline anti-malarial drugs inhibit spontaneous formation of beta-haematin (malaria pigment). FEBS Lett. **352**:54–57.
10. **Leed A, DuBay K, Ursos LMB, Sears D, de Dios AC, Roepe PD.** 2002. Solution structures of antimalarial drug-heme complexes. Biochemistry **41**:10245–10255.
11. **Cooper RA, Ferdig MT, Su XZ, Ursos LM, Mu J, Nomura T, Fujioka H, Fidock DA, Roepe PD, Wellems TE.** 2002. Alternative mutations at position 76 of the vacuolar transmembrane protein PfCRT are associated with chloroquine resistance and unique stereospecific quinine and quinidine responses in *Plasmodium falciparum.* Mol. Pharmacol. **61**:35–42.
12. **Griffin CE, Hoke JM, Samarakoon U, Duan J, Mu J, Ferdig MT, Warhurst DC, Cooper RA.** 2012. Mutation in the *Plasmodium falciparum* CRT protein determined the stereospecific activity of antimalarial *Cinchona* alkaloids. Antimicrob. Agents Chemother. **56**:5356–5364.
13. **Sidhu AB, Valderramos SG, Fidock DA.** 2005. *pfmdr1* mutations contribute to quinine resistance and enhance mefloquine and artemisinin sensitivity in *Plasmodium falciparum.* Mol. Microbiol. **57**:913–926.
14. **Ferdig MT, Cooper RA, Mu J, Deng B, Joy DA, Su XZ, Wellems TE.** 2004. Dissecting the loci of low-level quinine resistance in malaria parasites. Mol. Microbiol. **52**:985–997.
15. **Cooper RA, Lane KD, Deng B, Mu J, Patel JJ, Wellems TE, Su X, Ferdig MT.** 2007. Mutations in transmembrane domains 1, 4 and 9 of the *Plasmodium falciparum* chloroquine resistance transporter alter susceptibility to chloroquine, quinine and quinidine. Mol. Microbiol. **63**:270–282. (Erratum, **64**:1139–1148.).
16. **Roepe PD.** 2011. PfCRT-mediated drug transport in malarial parasites. Biochemistry **50**:163–171.
17. **Sidhu AB, Verdier-Pinard D, Fidock DA.** 2002. Chloroquine resistance in *Plasmodium falciparum* malaria parasites conferred by *pfcrt* mutations. Science **298**:210–213.
18. **Cabrera M, Paguio MF, Xie C, Roepe PD.** 2009. Reduced digestive vacuolar accumulation of chloroquine is not linked to resistance to chloroquine toxicity. Biochemistry **48**:11152–11154.
19. **Paguio MF, Bogle KL, Roepe PD.** 2011. *Plasmodium falciparum* resistance to cytocidal versus cytostatic effects of chloroquine. Mol. Biochem. Parasitol. **178**:1–6.
20. **Gorka AP, Alumasa JN, Sherlach KS, Jacobs LM, Nickley KB, Brower JP, de Dios AC, Roepe PD.** 2013. Cytostatic versus cytocidal activities of chloroquine analogues and inhibition of hemozoin crystal growth. Antimicrob. Agents Chemother. **57**:356–364.
21. **Karle JM, Karle IL, Gerena L, Milhous WK.** 1992. Stereochemical evaluation of the relative activities of the cinchona alkaloids against *Plasmodium falciparum.* Antimicrob. Agents Chemother. **36**:1538–1544.
22. **Warhurst DC, Craig JC, Adagu IS, Meyer DJ, Lee SY.** 2003. The relationship of physico-chemical properties and structure to the differential antiplasmodial activity of the cinchona alkaloids. Malaria J. **2**:26. doi: 10.1186/1475-2875-2-26.
23. **Dinio T, Gorka AP, McGinniss A, Roepe PD, Morgan JB.** 2012. Investigating the activity of quinine analogs versus chloroquine resistant *Plasmodium falciparum.* Bioorg. Med. Chem. **20**:3292–3297.
24. **Sidorowicz L, Skarzewski J.** 2011. Easy access to 9-epimers of *Cinchona* alkaloids: one-pot inversion by Mitsunobu esterification-saponification. Synthesis **5**:708–710.
25. **Trager W, Jensen JB.** 1976. Human malaria parasites in continuous culture. Science **193**:673–675.
26. **Bennett TN, Paguio M, Gligorijevic B, Seudieu C, Kosar AD, Davidson E, Roepe PD.** 2004. Novel, rapid, and inexpensive cell-based quantification of antimalarial drug efficacy. Antimicrob. Agents Chemother. **48**:1807–1810.
27. **Casabianca LB, An D, Natarajan JK, Alumasa JN, Roepe PD, Wolf C, de Dios AC.** 2008. Quinine and chloroquine differentially perturb heme monomer-dimer equilibrium. Inorg. Chem. **47**:6077–6081.
28. **Marques HM, Voster K, Egan TJ.** 1996. The interaction of the heme-octapeptide, N-acetylmicroperoxidase-8 with antimalarial drugs: solution studies and modeling by molecular mechanics methods. J. Inorg. Biochem. **64**:7–23.
29. **Ursos LM, DuBay KF, Roepe PD.** 2001. Antimalarial drugs influence the pH dependent solubility of heme via apparent nucleation phenomena. Mol. Biochem. Parasitol. **112**:11–17.
30. **Casabianca LB, de Dios AC.** 2004. ^{13}C NMR study of the self-association of chloroquine, amodiaquine, and quinine. J. Phys. Chem. A **108**:8505–8513.
31. **Evans DF.** 1959. The determination of the paramagnetic susceptibility of substances in solution by nuclear magnetic resonance. J. Chem. Soc., p 2003–2005.
32. **Bennett TN, Kosar AD, Ursos LM, Dzekunov S, Singh Sidhu AB, Fidock DA, Roepe PD.** 2004. Drug resistance-associated pfCRT mutations confer decreased *Plasmodium falciparum* digestive vacuolar pH. Mol. Biochem. Parasitol. **133**:99–114.
33. **Collier GS, Pratt JM, De Wet CR, Tshabalala CF.** 1979. Studies on haemin in dimethyl sulphoxide/water mixtures. Biochem. J. **179**:281–289.
34. **Caner H, Biedermann PU, Agranat I.** 2003. Conformational spaces of *Cinchona* alkaloids. Chirality **15**:637–645.